Article:

eprints@whiterose.ac.uk
https://eprints.whiterose.ac.uk/

Time-dependent probability density functions and information geometry in stochastic logistic and Gompertz models

Lucille-Marie Tenkès[1,2], Rainer Hollerbach[2] and Eun-jin Kim[3]

[1]*ENSTA ParisTech Université Paris-Saclay, 828,*

Boulevard des Maréchaux 91120 Palaiseau, France

[2]*Department of Applied Mathematics,*

University of Leeds, Leeds LS2 9JT, UK

[3]*School of Mathematics and Statistics,*

University of Sheffield, Sheffield, S3 7RH, UK

Abstract

A probabilistic description is essential for understanding growth processes far from equilibrium. In this paper, we compute time-dependent Probability Density Functions (PDFs) in order to investigate stochastic logistic and Gompertz models, which are two of the most popular growth models. We consider different types of short-correlated internal (multiplicative) and external (additive) stochastic noises and compare the time-dependent PDFs in the two models, elucidating the effects of the additive and multiplicative noises on the form of PDFs. We demonstrate an interesting transition from a unimodal to a bimodal PDF as the multiplicative noise increases for a fixed value of the additive noise. A much weaker (leaky) attractor in the Gompertz model leads to a significant (singular) growth of the population of a very small size. We point out the limitation of using stationary PDFs, mean value and variance in understanding statistical properties of the growth far from equilibrium, highlighting the importance of time-dependent PDFs. We further compare these two models from the perspective of information change that occurs during the growth process. Specifically, we define an infinitesimal distance at any time by comparing two PDFs at times infinitesimally apart and sum these distances in time. The total distance along the trajectory quantifies the total number of different states that the system undergoes in time, and is called the information length. We show that the time-evolution of the two models become more similar when measured in units of the information length and point out the merit of using the information length in unifying and understanding the dynamic evolution of different growth processes.

I.   INTRODUCTION

A variety of growth models are widely used in understanding the dynamic evolution of populations, not only in humans, ecology and biosystems, but also financial markets, environment, chemical and physical systems, etc. Two of the most popular models are the logistic and Gompertz models [1–5]. Mathematically, the utility of these models stems from the simplicity in which the growth is saturated to a finite value by a simple nonlinear damping term. Specifically, the logistic model for the variable x is governed by the following equation:

$$\frac{dx}{dt} = \gamma x (1 - \epsilon x), \tag{1}$$

which has the exact solution

$$x(t) = \frac{x_0}{\epsilon x_0 + (1 - \epsilon x_0) \exp(-\gamma t)}. \tag{2}$$

Here γ and $\gamma \epsilon$ are positive constants, representing the linear growth rate and nonlinear damping coefficient; x_0 is the value of x at $t = 0$. As t becomes large, Eq. (2) gives a stable solution $x = 1/\epsilon$ which corresponds to the carrying capacity; $x = 0$ is the unstable equilibrium point. The linear term γx can be considered to capture the overall effects (i.e. the birth rate minus death rate) that drive the growth while the nonlinear damping term $-\gamma \epsilon x^2$ slows down the growth and saturates x to the finite equilibrium value given by the carrying capacity $1/\epsilon$.

To compare the growth dynamics of x in the logistic model (1) with that governed by the Gompertz model, in this paper we opt to use a different variable y as follows:

$$\frac{dy}{dt} = \gamma y (1 - \epsilon \ln y). \tag{3}$$

In comparison with the logistic model, the Gompertz model for the variable y in Eq. (3) has a similar linear growth term γy but a different nonlinear damping $-\gamma \epsilon y \ln y$, which is weaker than the quadratic damping in the logistic model. Eq. (3) has the following exact solution:

$$y(t) = \exp\left[\frac{1}{\epsilon} - \left(\frac{1}{\epsilon} - \ln y_0\right) e^{-\epsilon \gamma t}\right], \tag{4}$$

2

where y_0 is the value of y at $t = 0$. As t becomes large, Eq. (4) gives a stable solution $y = e^{1/\epsilon}$, and $y = 0$ is the unstable equilibrium point. The specific equilibrium points $x(t \to \infty)$ and $y(t \to \infty)$ can easily be adjusted to take the same value in both models, for example by taking $\epsilon = 1/e$ for logistic and $\epsilon = 1$ for Gompertz, yielding e as the stable solution in both models. However, the strength and robustness of these equilibrium points in the presence of a stochastic noise can differ significantly due to the different nonlinear damping terms, as we will show in this paper.

The purpose of this paper is to investigate how these two models are affected by stochastic noise, which is now believed to be crucial in many systems [6–24]. For instance, variability has emerged to be a key factor in understanding the development of tumours [12–14]. Even when tumours may have smaller growth rates compared to normal cells [15], its growth will have significantly larger variation than normal cells. This variation increases with the complexity of the tumour as it progresses towards metastasis with the involvement of an increasing number of different processes on a broad range of scales, accompanied by the propagation of the loss of cellular stability on multiscales (e.g. [12–14]). Ultimately, the danger of a tumour is not measured simply by its average growth rate or variance, but by the rare occurrence of extreme events of such aggressive tumour growth (metastasis). These extreme events are the manifestation of intermittency, which is a generic feature in non-equilibrium systems (e.g. [16, 18]).

In the presence of such stochasticity and intermittency, a probabilistic description using a Probability Density Function (PDF), rather than relying on mean value and variance, becomes essential. Such PDFs would also enable us to understand the fundamental mechanisms responsible for bimodal distributions (e.g. [6]). Experimentally, obtaining a good quality of PDFs is often very challenging as it requires a sufficiently large number of simulations or observations. Therefore, a PDF is usually constructed by using data from a long time series, and in a technical term, is stationary (independent of time). Unfortunately, such stationary PDFs (averaged over time) miss crucial information about the dynamics/evolution of non-equilibrium processes (e.g. tumour evolution). Similar difficulty often arises in theoretical calculations due to analytical intractability, most previous work focusing on the computation of stationary PDFs. However, as the advancement

of experimental techniques (e.g. single-cell technology) enables us to access variability in tumour growth, different gene expression [6], cellular processes, etc., it is essential to predict time-dependent PDFs to improve our understanding of fundamental mechanisms determining the evolution of different distributions. Mathematically, in our growth models, a stochastic noise can appear either multiplicatively or additively, representing different types of internal or external noise.

In this paper, we calculate time-dependent PDFs in the stochastic logistic and Gompertz models and explore similarities and disparities between the two models. In particular, we demonstrate that stochastic noise can induce an interesting transition from unimodal to bimodal PDFs in both models as the attractor around the stable equilibrium point becomes leaky. For purely multiplicative noise, a much weaker (leaky) attractor in the Gompertz model is shown to lead to a much more significant (singular) growth of the population of a very small size. We show that time-dependent PDFs can drastically differ from stationary PDFs and that the variance is not a useful representation of the variability of a bimodal PDF, highlighting the importance of time-dependent PDFs, as well as other diagnostic quantities besides simply mean value and variance. We also present the geometric methodology to understand a growth process from the perspective of information change, and compare these two models in terms of information change. The latter is quantified by the information length which represents the total number of statistically different states that the system undergoes in time (see Section IV). This information length provides us with a useful system-independent method of understanding different stochastic processes to analyse different experimental data. In particular, we show that even though the time-evolution of the two models can be very different, they become more similar when measured in units of the information length. We also discuss implications of our results for bimodal variability in gene expression observed in single-cell experiments (e.g. [6]) and persisters (e.g. [25]).

The remainder of the paper is organised as follows. Section II introduces our stochastic logistic and Gompertz models. Section III presents exact analytic solutions for purely multiplicative noise, and shows that they develop exponentially growing (and correspondingly narrowing) peaks, as well as a singularity at the origin for the Gompertz model. Section IV

4

reviews the concept of information length, and applies it to the previous solutions. Section V considers the case of both multiplicative and additive noise, and shows how any non-zero additive noise regularises the previous solutions, and ensures that the final evolution is always toward a non-singular stationary distribution. Technical details of some of the derivations are also provided in two appendices.

II. STOCHASTIC LOGISTIC AND GOMPERTZ MODELS

To include stochastic noise in the logistic model, we consider the following Langevin equation:

$$\frac{dx}{dt} = (\gamma + \xi_1)x - \epsilon(\gamma + \xi_2)x^2 + \xi_3. \tag{5}$$

Here, as in Eq. (1), γ and $\gamma\epsilon$ are positive constants, representing the constant part of the growth rate and nonlinear damping coefficient. ξ_1 and ξ_2 are stochastic parts of these growth rate and damping coefficients. ξ_3 is an additive noise modelling fluctuations in the environment. We assume that ξ_i has zero mean value $\langle \xi_i \rangle = 0$, where angular brackets $\langle \rangle$ denote average over the stochastic noise. Furthermore, for simplicity, we assume that ξ_i ($i = 1, 2, 3$) are Gaussian noises with short correlation time and the following correlation function

$$\langle \xi_i(t)\xi_j(t') \rangle = D_{i,j}\delta(t - t'), \tag{6}$$

for $i = 1, 2, 3$. D_i represents the amplitude of the stochastic noise ξ_i, while D_{ij} represents the amplitude of the cross-correlation between ξ_i and ξ_j. The statistically independent noises ξ_i and ξ_j for $i \neq j$ are thus represented by $D_{ij} = 0$. Different cases of D_{ij} were studied in previous works, although they tend to be limited to stationary PDFs. In particular, bimodal stationary PDFs were shown for $D_{13} \neq 0$ and $\xi_2 = 0$ [3?]. The time-dependent PDFs were shown in our previous work for a linear model (i.e. $\epsilon = \xi_2 = \xi_3 = 0$) [26] and for a nonlinear model with $\xi_1 = \xi_3 = 0$ [26–28].

Similarly, as a generalisation of Eq. (3), we consider the following Langevin equation for the Gompertz model for a stochastic variable y:

$$\frac{dy}{dt} = (\gamma + \xi_1)y - \epsilon(\gamma + \xi_2)y \ln y + \xi_3. \tag{7}$$

5

Compared with the stochastic logistic model in Eq. (6), much less analysis has been done on the stochastic Gompertz model. We show later some of the challenges in obtaining solutions to Eq. (7) and the corresponding Fokker-Planck equation.

In the following, we consider two different cases of stochastic noises. Specifically, we investigate the case of the same multiplicative noise $\xi_1 = \xi_2 = \xi$ for the growth rate and nonlinear damping with no additive noise $\xi_3 = 0$ in Section III. We then include an independent additive noise $\xi_3 \neq 0$ with $D_{12} = D_{13} = 0$ in this model in Section V.

III. MULTIPLICATIVE NOISE ONLY ($\xi_1 = \xi_2 = \xi$ AND $\xi_3 = 0$)

In this section, we consider the case of the same multiplicative noise $\xi_1 = \xi_2 = \xi$ for the growth rate and nonlinear damping, with no additive noise $\xi_3 = 0$. This case $\xi_1 = \xi_2 = \xi$ is obtained in the limit of the strong correlation between ξ_1 and ξ_2 with $D_{11} = D_{22} = D_{12} \equiv D$. Therefore, Eq. (5) and (7) are reduced to

$$\frac{dx}{dt} = (\gamma + \xi)x(1 - \epsilon x), \tag{8}$$

$$\frac{dy}{dt} = (\gamma + \xi)y(1 - \epsilon \ln y). \tag{9}$$

In the seminal work by Kimura [2], Eq. (8) was used to model a random drift (selection) in population genetics. The Fokker-Planck equations corresponding to Eqs. (8) and (9) are as follows:

$$\partial_t p(x, t) = -\partial_x \left[\gamma x(1 - \epsilon x)p(x,t) \right] + D\partial_x \left[x(1 - \epsilon x)\partial_x [x(1 - \epsilon x)p(x,t)] \right], \tag{10}$$

$$\partial_t p(y, t) = -\partial_y \left[\gamma y(1 - \epsilon \ln y)p(y,t) \right] + D\partial_y \left[y(1 - \epsilon \ln y)\partial_y [y(1 - \epsilon \ln y)p(y,t)] \right]. \tag{11}$$

In the following section we will derive exact solutions to these two sets of Langevin and corresponding Fokker-Planck equations.

A. Time-dependent PDFs

We use the Stratonovich calculus [29–31], which recovers the limit of a short correlated forcing from the finite correlated forcing (e.g. [31]), and show how to obtain the exact solution for x and y and their time-dependent PDFs.

First, to solve Eq. (8), we divide it by $x(1 - \epsilon x)$:

$$\left[\frac{1}{x} + \frac{\epsilon}{1 - \epsilon x} \right] \frac{dx}{dt} = \gamma + \xi. \tag{12}$$

By integrating Eq. (12) over time, we obtain

$$\ln \left| \frac{x(1 - \epsilon x_0)}{(1 - \epsilon x)x_0} \right| = \gamma t + \Gamma(t), \tag{13}$$

or, alternatively,

$$x(t) = \frac{x_0}{\epsilon x_0 + (1 - \epsilon x_0) \exp\left(-\gamma t - \Gamma(t)\right)}, \tag{14}$$

where $\Gamma(t) = \int_0^t dt_1 \xi(t_1)$ is a Brownian motion. We note that the probability distribution function (PDF) of Γ is given by a Gaussian distribution with the zero mean value and the inverse temperature β as

$$p(\Gamma, t) = \sqrt{\frac{\beta}{\pi}} \exp\left[-\beta \Gamma^2\right], \tag{15}$$

where $\beta = 1/(4Dt)$ (e.g. [32]). β is related to the PDF's width or standard deviation σ as $\beta = 1/2\sigma^2$.

The probability distribution function of x is then obtained from Eq. (12) by using $p(x) = p(\Gamma) \left| \frac{d\Gamma}{dx} \right|$ and by expressing Γ in terms of x with the help of Eq. (14):

$$p(x, t) = \sqrt{\frac{\beta}{\pi}} \frac{1}{|x(1 - \epsilon x)|} \exp\left[-\beta \left(\ln \left| \frac{x(1 - \epsilon x_0)}{(1 - \epsilon x)x_0} \right| - \gamma t \right)^2 \right] \equiv \sqrt{\frac{\beta}{\pi}} \exp\left[-\phi\right], \tag{16}$$

where ϕ is defined as

$$\phi = \beta \left(\ln \left| \frac{x(1 - \epsilon x_0)}{(1 - \epsilon x)x_0} \right| - \gamma t \right)^2 + \ln |x(1 - \epsilon x)|. \tag{17}$$

Next, to solve Eq. (9), let $z = \ln y$ to recast it as

$$\frac{dz}{dt} = (\xi + \gamma)(1 - \epsilon z). \tag{18}$$

Again using the Stratonovich calculus [29–31], the solution is found to be

$$\frac{1}{\epsilon} \ln \left| \frac{1 - \epsilon z}{1 - \epsilon z_0} \right| = -\gamma t + \Gamma(t), \tag{19}$$

$$y = \exp \left[\frac{1}{\epsilon} - \left(\frac{1}{\epsilon} - \ln y_0 \right) e^{\epsilon[-\gamma t + \Gamma(t)]} \right], \tag{20}$$

7

where $z_0 = z(t = 0)$, $y_0 = y(t = 0)$, and $\Gamma(t) = \int_0^t dt_1\, \xi(t_1)$ is the Brownian motion.

To obtain the PDF $p(y, t)$, we first use the Gaussian PDF of $\Gamma(t)$ given in Eq. (15) and the conservation of the probability $p(z, t) = p(\Gamma) \left| \frac{d\Gamma}{dz} \right|$ together with $\left| \frac{d\Gamma}{dz} \right| = \frac{1}{|1 - \epsilon z|}$ to obtain

$$p(z, t) = \sqrt{\frac{\beta}{\pi}} \frac{1}{|1 - \epsilon z|} \exp\left[-\beta \left(\frac{1}{\epsilon} \ln \left| \frac{1 - \epsilon z}{1 - \epsilon z_0} \right| + \gamma t \right)^2 \right]. \tag{21}$$

We then use the conservation of the probability again as $p(y, t) = p(z, t) \left| \frac{dz}{dy} \right|$ and $\frac{dz}{dy} = \frac{1}{y}$ (recall $z = \ln y$) to obtain

$$p(y, t) = \sqrt{\frac{\beta}{\pi}} \frac{1}{|y(1 - \epsilon \ln y)|} \exp\left[-\beta \left(\frac{1}{\epsilon} \ln \left| \frac{1 - \epsilon \ln y}{1 - \epsilon \ln y_0} \right| + \gamma t \right)^2 \right] \equiv \sqrt{\frac{\beta}{\pi}} \exp\left[-\psi \right], \tag{22}$$

where ψ is defined as

$$\psi = \beta \left(\frac{1}{\epsilon} \ln \left| \frac{1 - \epsilon \ln y}{1 - \epsilon \ln y_0} \right| + \gamma t \right)^2 + \ln |y(1 - \epsilon \ln y)|. \tag{23}$$

To summarize, Eqs. (16) and (22) are derived as the PDFs of the Langevin equations (8) and (9), and are correspondingly also exact solutions of the Fokker-Planck equations (10) and (11) respectively (as can also be verified by direct substitution back into these equations). Both solutions represent the evolution of δ-functions initially located at x_0 and y_0, respectively.

Figure 1 shows examples of the subsequent evolution. Here and throughout the remainder of this paper we fix $\gamma = 1$ for both processes, and $\epsilon = 1/e$ for logistic and $\epsilon = 1$ for Gompertz to ensure that both models have the same stable equilibrium point e in the absence of the stochastic noise. Our expectation therefore is that solutions should evolve toward the stable equilibrium at e. As seen in Figure 1, for small D this is indeed the case; the δ-functions initially located at $x_0 = y_0 = 0.8$ move monotonically toward e. In the intermediate stages of the evolution they also broaden considerably, but once they approach e they become increasingly narrow again.

In contrast, for larger D the peaks hardly move at all, but instead become so broad that they fill essentially the entire interval $(0, e)$. Once they sense the presence of the equilibrium at 0, they also begin to form peaks there, even though 0 is an *unstable* point of the original equations (1) and (3). Indeed, for the Gompertz model the peak at the origin is clearly far stronger than the peak at e. For the logistic model the peaks are more comparable, and Figure 1 is inconclusive regarding which one is ultimately dominant.
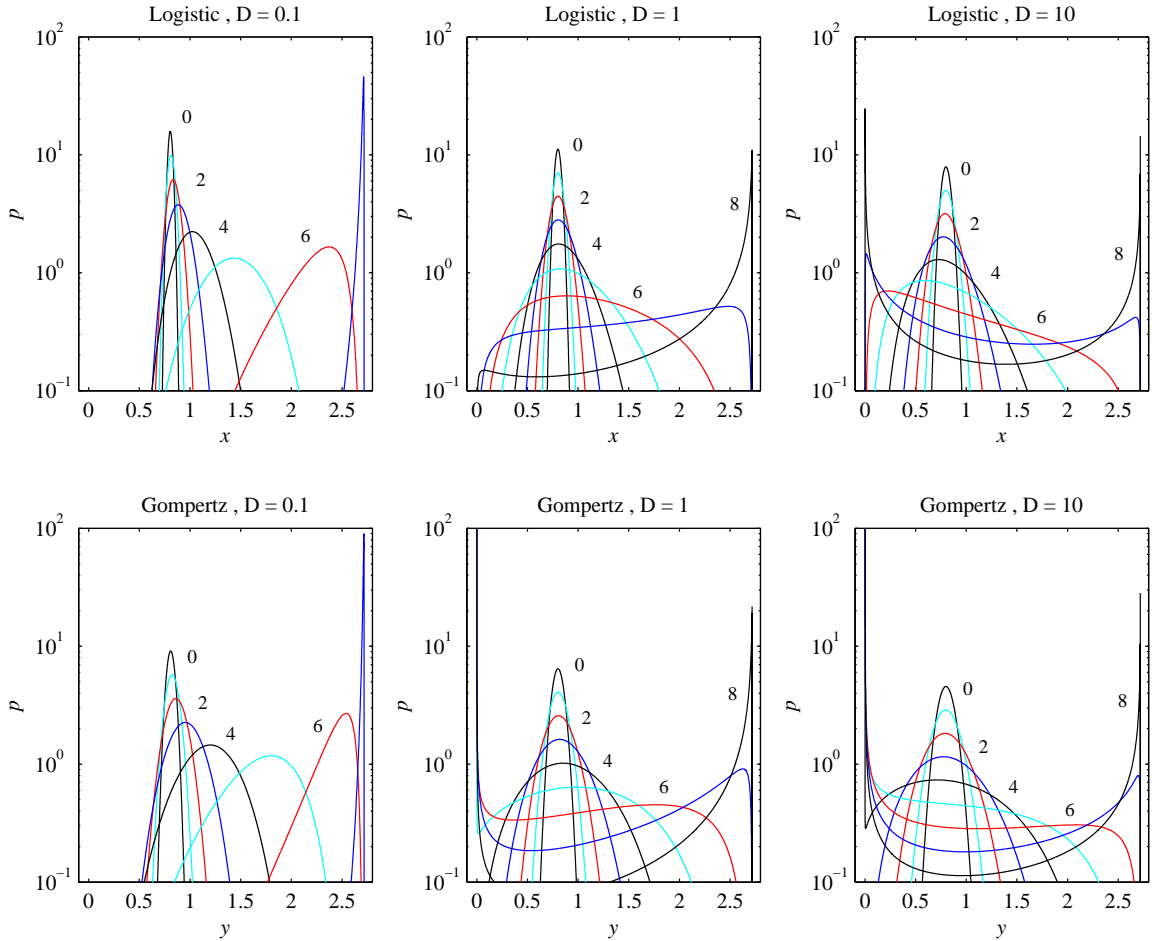
8

FIG. 1: Illustrations of the analytic expressions (16) for the logistic model in the top row, and (22) for the Gompertz model in the bottom row. From left to right $D = 0.1$, 1 and 10 as indicated. The δ-functions are initially located at $x_0 = y_0 = 0.8$. The numbers beside individual curves indicate time: For $D = 0.1$ these are given by $t = 0.01 \cdot 2.5^n$, $n = 0 - 7$ (so $t = 0.01 - 6.1$), for $D = 1$, $t = 0.002 \cdot 2.5^n$, $n = 0 - 8$ (so $t = 0.002 - 3$), and for $D = 10$, $t = 0.0004 \cdot 2.5^n$, $n = 0 - 8$ (so $t = 0.0004 - 0.61$).

B. Behaviour of Peaks near $x = y = e$ and $x = y = 0$

We clearly need to better understand the behaviour of these solutions (16) and (22), and especially this somewhat counter-intuitive behaviour that for sufficiently large D they become bimodal, yielding peaks not only at the (expected) stable point e, but also at the unstable point 0.

We begin with the logistic model (16), and investigate its behaviour near e. If we let

$x = e - \delta x$ and expand the various terms in ϕ in Eq. (17) to first order in δx we obtain

$$\phi \approx \beta \left(\ln \left| \frac{(1 - \epsilon x_0)}{\epsilon^2 \, \delta x \, x_0} \right| - \gamma t \right)^2 + \ln (\delta x). \tag{24}$$

The location of the PDF peak will occur at that x where $\partial_x p(x,t) = 0 = \partial_x \phi$, so differentiating (24) gives us the motion of the peak position as

$$\frac{\partial \phi}{\partial x} \approx -2\beta \left(\ln \left| \frac{(1 - \epsilon x_0)}{\epsilon^2 \, \delta x \, x_0} \right| - \gamma t \right) \frac{1}{\delta x} + \frac{1}{\delta x} = 0, \tag{25}$$

which yields

$$\delta x_s \approx \frac{1 - \epsilon x_0}{\epsilon^2 x_0} e^{-\left(\gamma t + \frac{1}{2\beta}\right)} = \frac{e(e - x_0)}{x_0} e^{-(2D+1)t}, \tag{26}$$

where we have again used $\beta = 1/4Dt$, $\gamma = 1$ and $\epsilon = 1/e$ for the logistic model. With the position of the peak known, it is then straightforward to evaluate the PDF at that position to obtain

$$p(e - \delta x_s, t) = \sqrt{\frac{1}{4\pi Dt}} \frac{x_0}{e(e - x_0)} e^{(D+1)t}. \tag{27}$$

To consider the logistic model near the origin, we follow much the same procedure, except that we expand in x itself rather than in δx. The results are

$$\phi \approx \beta \left(\ln \left| \frac{x(1 - \epsilon x_0)}{x_0} \right| - \gamma t \right)^2 + \ln x, \tag{28}$$

so again setting the derivative to zero yields

$$\frac{\partial \phi}{\partial x} \approx 2\beta \left(\ln \left| \frac{x(1 - \epsilon x_0)}{x_0} \right| - \gamma t \right) \frac{1}{x} + \frac{1}{x} = 0, \tag{29}$$

$$x_u \approx \frac{x_0}{1 - \epsilon x_0} e^{\left(\gamma t - \frac{1}{2\beta}\right)} = \frac{e x_0}{e - x_0} e^{-(2D-1)t}, \tag{30}$$

and the amplitude is finally given by

$$p(x_u, t) = \sqrt{\frac{1}{4\pi Dt}} \frac{e - x_0}{e x_0} e^{(D-1)t}. \tag{31}$$

If we then compare the peak amplitudes (27) and (31), we see that the peak at the stable point $x = e$ will always dominate for sufficiently large t, since it has the larger exponential growth rate. Nevertheless, for $D > 1$ the peak at the unstable point $x = 0$ will also grow, indicating the transition from a unimodal to a bimodal PDF. That is, a sufficiently
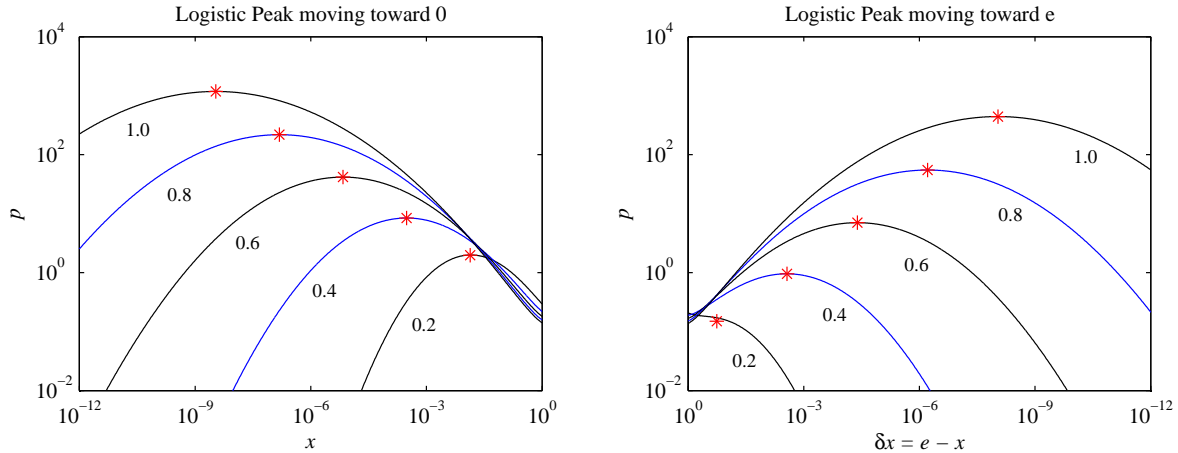
FIG. 2: The five curves in each panel correspond to the exact logistic solution (16), with $D = 10$ and $x_0 = 0.5$, at the times indicated by the numbers beside each curve. The asterisks denote the asymptotic formulas, (30) and (31) for the approach to 0 in the left panel, and (26) and (27) for the approach to e in the right panel. Note how each asterisk is indeed in near perfect agreement with the top of its corresponding curve.

strong multiplicative noise promotes a growth of the population (x) of small size around the unstable equilibrium point.

Finally, if we compare the multiplicative factors, $x_0/e(e - x_0)$ for the peak at e versus $(e - x_0)/ex_0$ for the peak at 0, we see that even these are intuitively understandable: an x_0 close to e means the e-peak has a larger factor, whereas an x_0 close to 0 means the 0-peak has a larger factor. Figure 2 shows how these asymptotic formulas compare with the exact expression, and shows that even quite modest t values already yield excellent agreement. Other choices of D and/or x_0 yielded similarly good agreement. We conclude therefore that the behaviour of Eq. (16) is fully understood.

The Gompertz peak moving toward e can be analysed in exactly the same way. If we let $y = e - \delta y$ and expand ψ in Eq. (23) to first order in δy, the final results are

$$\delta y_s \approx e(1 - \ln y_0)e^{-\epsilon\left(\gamma t + \frac{1}{2\beta}\right)} = e(1 - \ln y_0)e^{-(2D+1)t}, \tag{32}$$

$$p(e - \delta y_s, t) = \sqrt{\frac{1}{4\pi Dt}} \frac{1}{e(1 - \ln y_0)} e^{(D+1)t}. \tag{33}$$

It is interesting to note that the exponential factors $e^{-(2D+1)t}$ and $e^{(D+1)t}$ are both exactly the same as for the logistic peak moving toward e. The stable equilibrium point is evidently insensitive to the precise form of the nonlinear terms in the original Langevin equations.

11

The agreement between the exact solution (22) and these asymptotic formulas (32) and (33) is also much the same as for the logistic peaks in Figure 2.

In contrast, the behaviour of the Gompertz solution (22) near the origin is radically different. Instead of a peak moving toward the origin, there is a powerful singularity that starts at the origin and moves inward. To see this, we begin by evaluating $\frac{dp}{dy}$, setting it equal to 0, and solving for t. The result is

$$t = -\ln \left(\frac{1 - \ln y}{1 - \ln y_0} \right) \Big/ (1 + 2D \ln y). \tag{34}$$

If this equation could be inverted for y as a function of t, it would give an expression for the movement of any peaks (or troughs). However, even without being able to invert for $y(t)$, by simply graphing $t(y)$ we can still track the peaks and troughs.

Figure 3 shows representative examples, for $D = 1$, and three y_0 values. Starting with the simplest case, for $y_0 = 0.7$ the original δ-function moves monotonically outward, eventually approaching e in precise agreement with Eq. (32). Additionally, there is a trough that originates from $y \to 0$, and eventually asymptotes to $y = e^{-1/2D}$ (where the denominator of Eq. (34) is zero). The first panel in the bottom row of Figure 3 shows the corresponding PDFs, which indeed exhibit peaks and troughs exactly as predicted by the first panel in the top row.

Turning next to $y_0 = 0.5$, the two solution tracks of Eq. (34) now connect differently. The initial δ-function peak combines with the trough coming from $y \to 0$, destroying both. There is then an intermediate time $0.195 < t < 0.525$ (for these particular D and y_0 values) where there are neither peaks nor troughs, and $p(y, t)$ is monotonic. Finally, for $t > 0.525$ a new solution track emerges, with the peak again approaching e, and the trough approaching $e^{-1/2D}$. The third panel in the bottom row of Figure 3 again shows the corresponding PDFs; note especially the monotonic behaviour at the intermediate time.

Finally, the middle panels in Figure 3 show the transition point from one regime to the other. For $y_0 > e^{-1/2D}$ the solution tracks are like the $y_0 = 0.7$ case, for $y_0 < e^{-1/2D}$ they are like the $y_0 = 0.5$ case, and for $y_0 = e^{-1/2D}$ (≈ 0.61 for $D = 1$) they are as indicated in the middle panel.

For large t we see therefore that the behaviour is always the same: there is a peak approaching e as described by Eq. (32), and there is a trough approaching $e^{-1/2D}$ from either the left or the right, depending on whether y_0 is less than or greater than this value.
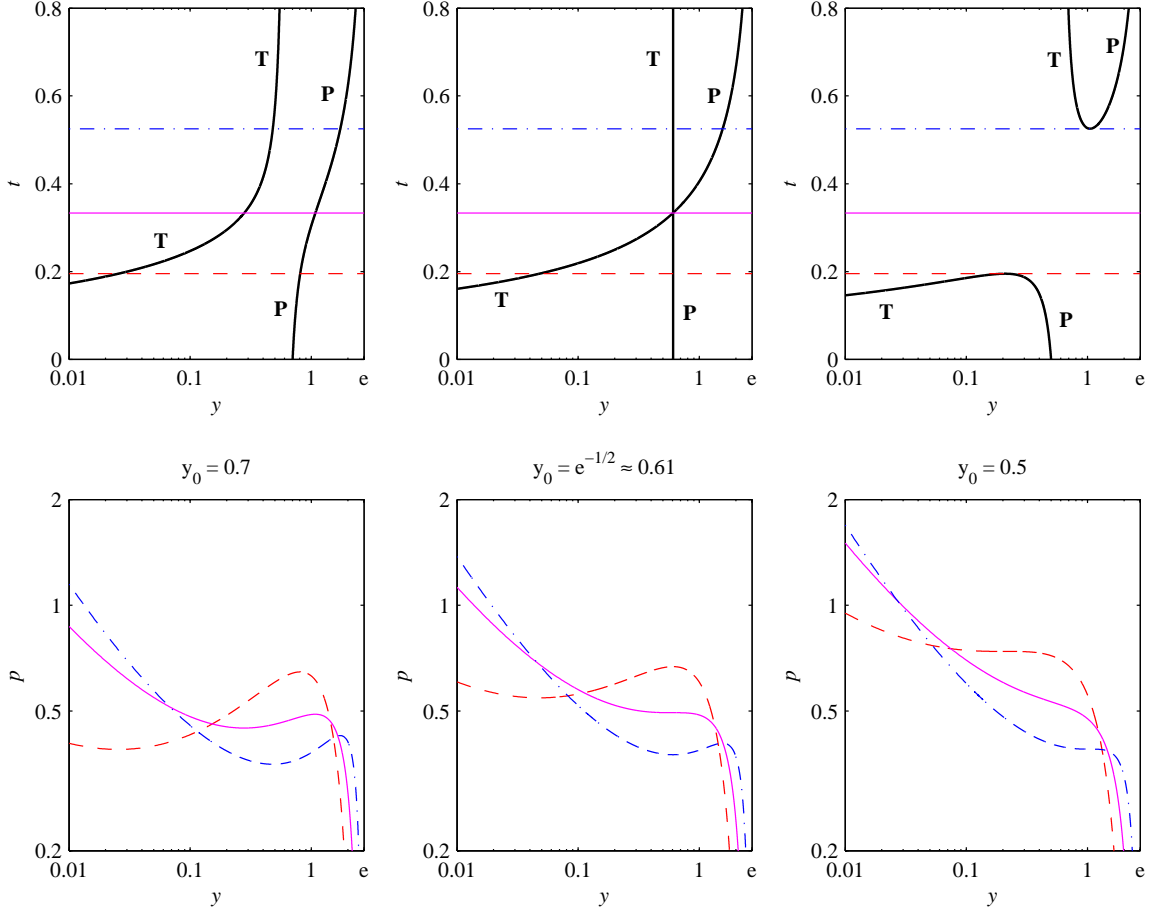
FIG. 3: The thick black lines in the top row plot Eq. (34), showing the locations in time of any peaks or troughs, indicated by the letters **P** and **T**. From left to right $y_0 = 0.7$, 0.61 and 0.5, and $D = 1$ for all three. The thin horizontal lines are at $t = 0.195$, 0.333 and 0.525, with the corresponding PDFs shown in the bottom row. Note how the peaks and troughs (or lack thereof) agree with the predictions in the top row. Note finally how the $t = 0.525$ PDFs especially are strongly suggestive of a $p \sim y^a$ scaling, with $a < 0$, indicating a singularity at the origin.

The final point to understand then is the trough emerging from the $y \to 0$ regime, and what $p(y, t)$ ultimately looks like in this regime. We begin by noting that because Eq. (34) has $\lim_{y \to 0} t = 0$, whatever singular behaviour emerges from this region happens *instantaneously*, as soon as $t > 0$.

To see what $p(y, t)$ looks like for $y \to 0$, we note that the bottom row of Figure 3 suggests a scaling of the form $p \sim y^a$, with $a < 0$. This in turn suggests examining the quantity $\frac{y}{p} \frac{dp}{dy}$; if p were exactly of the form y^a, then a would equal exactly this quantity. From (22) we
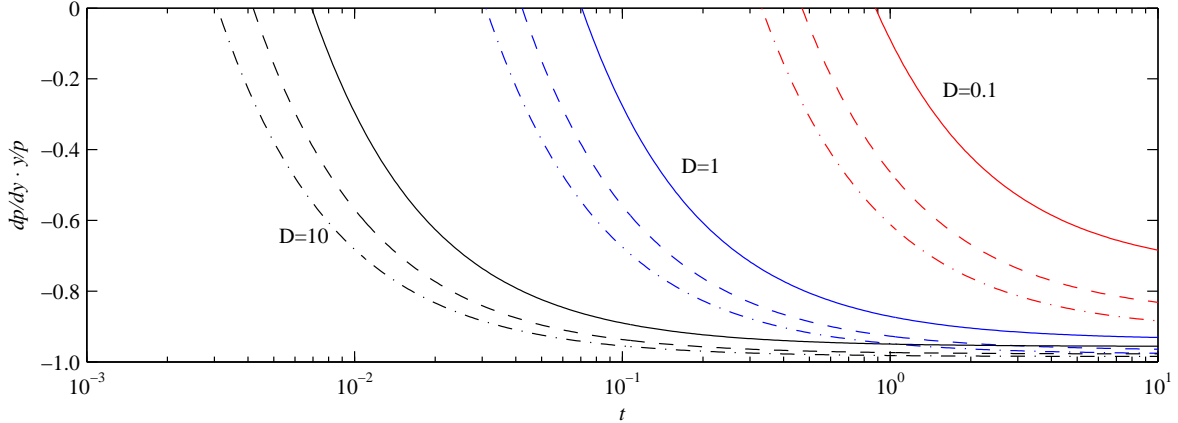
13

FIG. 4: The quantity $\alpha = \frac{y}{p}\frac{dp}{dy}$ in Eq. (35) as a function of time, for $D = 0.1$, 1 and 10 as indicated, and $y = 10^{-10}$ (solid), 10^{-20} (dashed), and 10^{-30} (dash-dotted). Note in particular how α becomes negative for all combinations of parameters, and how this happens earliest for $y \to 0$. The initial peak is fixed at $y_0 = 1$; other values yield qualitatively the same behaviour.

obtain

$$\alpha = \frac{y}{p}\frac{dp}{dy} = -\frac{\ln\left(\frac{1-\ln y}{1-\ln y_0}\right) + (1 + 2D\ln y)t}{(1 - \ln y)2Dt}. \tag{35}$$

To interpret this result, we first note that α depends on y, indicating that p is not exactly of the form y^α. However, because y enters into α only as $\ln y$, the dependence is very weak, and locally p is closely approximated by y^α. Figure 4 shows α as a function of t, for $D = 0.1$, 1 and 10, and $y = 10^{-10}$, 10^{-20} and 10^{-30}. For all combinations we find that α becomes negative once $t > O(D^{-1})$. Indeed, if we are interested in the true $y \to 0$ limit, we find $\alpha \to -1$ for all $t > 0$. So again, the singularity at the origin starts instantaneously, and propagates outward to ever larger y as t increases, with

$$\lim_{t\to\infty} \alpha = \frac{1/2D + \ln y}{1 - \ln y}. \tag{36}$$

Note how this quantity varies between -1 for $y \to 0$ and 0 for $y = e^{-1/2D}$, where it coincides with the previously understood behaviour of the trough at that location. For all y to the left of that trough therefore p is monotonically increasing, and indeed approaching ever closer to a y^{-1} singularity at the origin. (Because α never reaches -1 for any non-zero y though, the integral $\int_0^\infty p\,dy$ not only converges, but always remains 1, as required by conservation of total probability.)

14

IV.   INFORMATION LENGTH

In this section, we show how to utilise PDFs to understand information change in general, and then apply these concepts to our logistic and Gompertz PDFs. First, for any given two PDFs, we quantify the difference between them by assigning an appropriate metric to probability such that the distance increases with the difference between the two PDFs. This metric provides an interesting link between stochastic processes and associated geometric structure. A key characteristic of non-equilibrium processes is however in its variability in time (or space), reflected in the temporal change in PDFs, time-varying PDFs implying the change in information content in the system. In this case, we define an infinitesimal distance at any time by comparing two PDFs at times infinitesimally apart and sum these distances in time. The total distance along the trajectory of the system quantifies the total number of different states that the system undergoes in time, and is called the information length [27, 28, 33–35].

To show this explicitly, we consider a stochastic variable z and suppose that we can compute its time-dependent PDFs $p(z,t)$ either analytically or numerically in the case where its governing equation is known, or otherwise construct $p(z,t)$ from experimental/observational data. Defining the information length involves two steps [27, 28, 33–36]: First we need to compute the dynamic time unit $\tau(t)$, which is the characteristic timescale over which $p(z,t)$ temporally changes *on average* at time t. Second, we need to compute the total elapsed time in units of this $\tau(t)$. As done in [27, 28, 33–36], we compute τ by utilising the following second moment $\mathcal{E}$:

$$\mathcal{E} \equiv \frac{1}{[\tau(t)]^2} = \int dz \frac{1}{p(z,t)} \left[\frac{\partial p(z,t)}{\partial t} \right]^2. \tag{37}$$

We note that $\mathcal{E}$ is the root-mean-square fluctuating energy for a Gaussian PDF (see [28]). As defined in Eq. (37), τ has dimensions of time, and quantifies the correlation time over which $p(z,t)$ changes, thereby serving as the time unit in statistical space. Alternatively, $1/\tau$ quantifies the (average) rate of change of information in time. We recall that $\tau(t)$ in Eq. (37) is related to the second derivative of the relative entropy (or Kullback-Leibler divergence) (see Appendix A and [27]).

The total accumulated change in information between the initial and final times, 0 and t respectively, is defined by measuring the total elapsed time in units of τ as:

$$\mathcal{L}(t) = \int_0^t dt_1 \sqrt{\mathcal{E}(t_1)} = \int_0^t \frac{dt_1}{\tau(t_1)} = \int_0^t dt_1 \sqrt{\int dz \frac{1}{p(z,t_1)} \left[\frac{\partial p(z,t_1)}{\partial t_1} \right]^2}. \qquad (38)$$

Eq. (38) provides the total number of different states that a system passes through from the initial state with the PDF $p(z,0)$ at time 0 to the final state with the PDF $p(z,t)$ at time t, establishing a distance between the initial and final PDFs in the statistical space. For example, in equilibrium where $\frac{\partial p}{\partial t} = 0$, $\mathcal{E} = 0$ and hence $\tau(t_1) \to \infty$ for all time t_1. Measuring dt_1 in units of this infinite $\tau(t_1)$ at any t_1, $dt_1/\tau(t_1) = 0$ in Eq. (38), and thus $\int_0^t dt_1/\tau(t_1) = 0$. This can be viewed as asserting that in statistical space there is no flow of time in equilibrium. In the opposite limit, large $\mathcal{E}$ corresponds to small τ, meaning that information changes very quickly in dimensional time. See Appendix A for the interpretation of $\mathcal{L}$ from the perspective of the infinitesimal relative entropy.

Our information length is based on Fisher information (c.f. [37]) and is a generalisation of statistical distance [38], where the distance is set by the number of distinguishable states between two PDFs. While the latter was heavily used in equilibrium or near-equilibrium of classical and quantum systems (e.g. [39, 40]), our recent work [27, 28, 33–36] adapted this concept to a non-equilibrium system to elucidate geometric structure of non-equilibrium processes. Specifically, [35] mapped out the attractor structure $\mathcal{L}_\infty$ vs z_0 for linear and cubic processes and showed that a linear damping preserves a linear geometry $\mathcal{L}_\infty \propto z_0$ whereas a nonlinear damping gives rise to a power-law scaling $\mathcal{L}_\infty \propto z_0^n$ ($n \sim 1.5 - 1.9$) of the attractor structure. [28] found interesting geodesic solutions in a non-autonomous Ornstein-Uhlenbeck (O-U) process [32] by modulating model parameters and by including time-dependent external deterministic killing term. Notably, the modulation of the model parameters and the killing term were periodic/oscillatory. [35, 36] reported the asymmetry in $\mathcal{L}$ in order-to-disorder versus disorder-to-order transitions.

To now apply these general ideas to our particular models here, we begin with the analytical derivation of $\mathcal{E}$ and $\mathcal{L}$ for the Gompertz model (22). To derive $\mathcal{E}$ defined in Eq. (37),

16

we let $z = \ln y$ and use Eq. (21) to obtain:

$$\partial_t p(z,t) = \left\{ \dot\beta \left[\frac{1}{2\beta} - \Gamma(t)^2 \right] - 2\gamma\beta\Gamma(t) \right\} p(z,t), \tag{39}$$

where $\Gamma(t) = \int_0^t dt_1\, \xi(t_1) = \frac{1}{\epsilon} \ln \frac{1-\epsilon z_0}{1-\epsilon z} - \gamma t$ is the Brownian motion. Using Eq. (39), we then obtain

$$
\begin{aligned}
\mathcal{E} &= \int \frac{(\partial_t p(y,t))^2}{p(y,t)} dy = \int \frac{(\partial_t p(z,t))^2}{p(z,t)} dz \\
&= \dot\beta^2 \left\langle \left(\frac{1}{2\beta} - \Gamma^2 \right)^2 \right\rangle - 4\gamma\beta \left\langle \Gamma \left(\frac{1}{2\beta} - \Gamma^2 \right)^2 \right\rangle + 4\gamma^2\beta^2 \left\langle \Gamma^2 \right\rangle \\
&= \dot\beta^2 \left[\frac{1}{4\beta^2} - \frac{1}{2\beta^2} + \frac{3}{4\beta^2} \right] + 2\gamma^2\beta = \frac{\dot\beta^2}{2\beta^2} + 2\gamma^2\beta = \frac{\dot\beta^2}{2\beta^2} + 2\beta \langle \dot z \rangle^2.
\end{aligned} \tag{40}
$$

Here we used $\langle \dot z \rangle = \gamma$, $\langle \Gamma \rangle = \langle \Gamma^3 \rangle = 0$, $\langle \Gamma^2 \rangle = 1/2\beta$, and $\langle \Gamma^4 \rangle = 3\langle \Gamma^2 \rangle$. It is interesting to note that in terms of the inverse temperature β and the mean value $\langle z \rangle$, $\mathcal{E}$ in Eq. (40) takes the same form as for $\mathcal{E}$ in the Ornstein-Uhlenbeck process [32]. Using $\beta = 1/4Dt$ for our model, we simplify Eq. (40) as follows:

$$\mathcal{E} = \frac{1}{2\beta^2} \left(\frac{\beta}{t} \right)^2 + 2\gamma\beta = \frac{1}{2t^2} + 2\gamma\beta = \frac{1}{2t^2} \left(1 + \frac{\gamma}{D} t \right). \tag{41}$$

By using the definition of $\mathcal{L}(t_i, t_f) = \int_{t_i}^{t_f} dt_1 \sqrt{\mathcal{E}(t_1)}$ given in Eq. (38) and using Eq. (41), we obtain $\mathcal{L}$ in the following form:

$$\mathcal{L}(t) = \int_{t_i}^{t_f} dt \frac{1}{\sqrt{2}t} \sqrt{1 + \overline\gamma t}, \tag{42}$$

where $\overline\gamma = \gamma/D$. We let $T = \sqrt{1 + \overline\gamma t}$ and $T_i = T(t = t_i)$ and $T_f = T(t = t_f)$ and use the change of variables to evaluate Eq. (42) as follows:

$$
\begin{aligned}
\mathcal{L} &= \frac{2}{\gamma} \int_{T_i}^{T_f} dT\, T \frac{\gamma}{\sqrt{2}} \frac{T}{T^2 - 1} = \sqrt{2} \int_{T_i}^{T_f} dT \left[1 + \frac{1}{T^2 - 1} \right] \\
&= \sqrt{2} \left[T + \frac{1}{2} \ln \frac{T-1}{T+1} \right]_{T_i}^{T_f} = \sqrt{2} \left\{ T_f - T_i + \frac{1}{2} \ln \left[\frac{T_f - 1}{T_f + 1} \frac{T_i + 1}{T_i - 1} \right] \right\},
\end{aligned} \tag{43}
$$

where $T_i = \sqrt{1 + \gamma t_i/D}$ and $T_f = \sqrt{1 + \gamma t_f/D}$.

Next, we show that *identical* results are obtained for the stochastic logistic model by following similar analysis as above. First, from Eq. (16), we obtain

$$\partial_t p(x,t) = \left\{ \dot\beta \left[\frac{1}{2\beta} - \Gamma^2 \right] - 2\gamma\beta\Gamma \right\} p(x,t), \tag{44}$$

17

where $\Gamma(t) = \int_0^t dt_1\, \xi(t_1) = \ln\frac{(1-\epsilon x_0)x}{(1-\epsilon x)x_0} - \gamma t$ is the Brownian motion. Thus,

$$
\begin{aligned}
\mathcal{E} &= \int \frac{(\partial_t p(x))^2}{p(x)} dx = \dot\beta^2 \left\langle \left(\frac{1}{2\beta} - \Gamma^2\right)^2 \right\rangle - 4\gamma\beta \left\langle \Gamma\left(\frac{1}{2\beta} - \Gamma^2\right)^2 \right\rangle + 4\gamma^2\beta^2 \left\langle \Gamma^2\right\rangle \\
&= \frac{\dot\beta^2}{2\beta^2} + 2\gamma^2\beta = \frac{1}{2t^2}\left(1 + \frac{\gamma}{D}t\right),
\end{aligned}
\tag{45}
$$

where again $\beta = 1/4Dt$, which is the same as Eq. (40). Eq. (45) thus leads to the same information length $\mathcal{L}$ as in Eq. (43).

It is quite extraordinary that two processes as different as the logistic and Gompertz models should nevertheless have exactly the same functions $\mathcal{E}(t)$ and $\mathcal{L}(t)$. This is due to the fact that Eqs. (8) and (9) can be mapped into a similar Gaussian process by a suitable change of variables. Another interesting – and *a priori* not obvious – point is that the initial positions x_0 and y_0 do not enter into these expressions. All peaks starting anywhere for either model have the same $\mathcal{L}(t)$, with D being the only remaining parameter. Figure 5 shows the results. For t up to $O(1)$, $\mathcal{L}$ is independent of D, and scales as $\ln t$. (This also means that $t_i = 0$ should not be used in Eq. (43); the value used here is $t_i = 10^{-5}$.) For sufficiently large t we recover the $\sqrt{t/D}$, in agreement of the scaling predicted in (43). This independence of $\mathcal{L}$ on x_0 and y_0 can be traced back to the fact that the movement of the PDF peak in the transformed Gaussian process is a drift, which is independent of the position, in a sharp contrast to the movement of PDF peak in the O-U process caused by the position-dependent frictional force. These results thus reveal the merit of using the information length in unifying different stochastic processes.

Finally, if we return briefly to Figure 1, two points stand out: First, the entire evolution shown in Figure 1 occurs in this $t \le O(1)$ regime. The $\sqrt{t/D}$ scaling obtained for $t > O(1)$ therefore only applies to peaks that are already so narrow that they would be unlikely to be relevant to real-world data. Second, we recall that the curves shown in Figure 1 are at times $t = t_0 \cdot 2.5^n$, $n = 0, 1, \ldots$. The $\mathcal{L} \approx 0.71\ln(t/t_i)$ scaling for small t then implies that the information length between successive PDFs is roughly constant, around $0.71\ln 2.5 = 0.65$. In fact, the time $t = t_0 \cdot 2.5^n$, $n = 0, 1, \ldots$ in Figure 1 was chosen precisely to show the evolution of a PDF with the equal increment of $\mathcal{L}$, so that the two PDFs at the two subsequent times have the same change in information. Figure 1 shown at equal
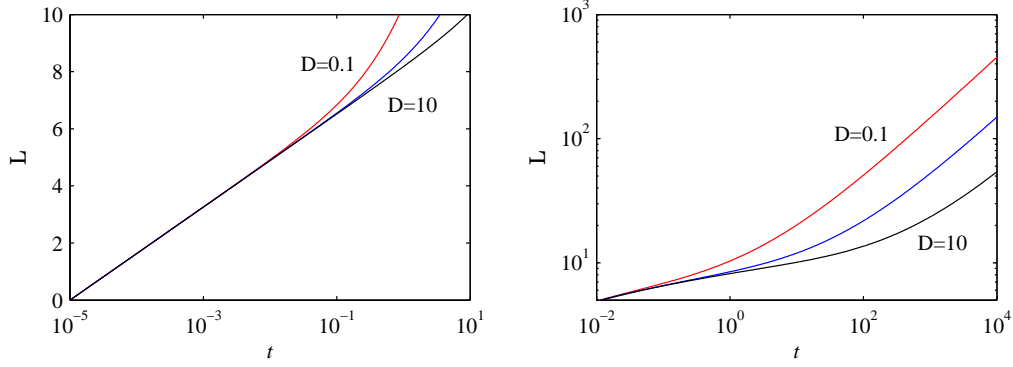
FIG. 5: $\mathcal{L}(t)$ according to Eq. (43), for $D = 0.1$, 1 and 10 as indicated. The left panel shows the $\ln t$ small-time behaviour; the right panel shows the $\sqrt{t/D}$ large-time behaviour.

increments of time would look very different, and much less informative as some of the PDFs would look very similar while others would look drastically different. This highlights another advantage of using the information length in understanding information flow and true dynamical change in non-equilibrium processes.

V. MULTIPLICATIVE AND ADDITIVE NOISE ($\xi_1 = \xi_2 = \xi$ AND $\xi_3 \neq 0$)

We saw in section III that the models with only internal but no external noise never form stationary PDFs, but instead form ever sharper peaks, eventually becoming so narrow that they are hardly relevant to most real situations. In this section we therefore extend these models to include an additive noise $\xi_3 \equiv \eta$, which can represent either external noise or random mutation rates (e.g. [4]). In this case, Eqs. (5) and (7) take the form:

$$\frac{dx}{dt} = (\gamma + \xi)x(1 - \epsilon x) + \eta, \tag{46}$$

$$\frac{dy}{dt} = (\gamma + \xi)y(1 - \epsilon \ln y) + \eta, \tag{47}$$

where we again use strongly correlated noises $\xi_1 = \xi_2 = \xi$ with $D_{11} = D_{22} = D_{12} \equiv D$, while we assume $\xi_3 = \eta$ is uncorrelated with ξ, so $D_{13} = D_{23} = 0$ and $D_{33} \equiv D_3$. The Fokker-Planck equations corresponding to Eqs. (46) and (47) are then:

$$\partial_t p = -\partial_x \left[\gamma x(1 - \epsilon x)p\right] + D\partial_x \left[x(1 - \epsilon x)\partial_x[x(1 - \epsilon x)p]\right] + D_3\partial_{xx}p, \tag{48}$$

$$\partial_t p = -\partial_y \left[\gamma y(1 - \epsilon \ln y)p\right] + D\partial_y \left[y(1 - \epsilon \ln y)\partial_y[y(1 - \epsilon \ln y)p]\right] + D_3\partial_{yy}p. \tag{49}$$

19

Because the second-derivative terms are now strictly positive, diffusion will prevent infinitely sharp gradients from forming, and the solutions will instead ultimately equilibrate to stationary distributions. One key question is then to what extent the previous unimodal versus bimodal behaviour remains the same once D_3 is added to the problem.

A. Logistic stationary distribution

For the logistic model it is possible to derive the following analytic expression for the stationary solutions to Eq. (48):

$$p(x) = \frac{1}{\sqrt{D(x - \epsilon x^2)^2 + D_3}} \exp\left\{ \frac{\gamma}{4D} \left[\frac{1}{c_1} \ln\left| \frac{z + c_1/\epsilon}{z - c_1/\epsilon} \right| + \frac{1}{c_2} \ln\left| \frac{z + c_2/\epsilon}{z - c_2/\epsilon} \right| \right] \right\},$$

$$= \frac{1}{\sqrt{D(x - \epsilon x^2)^2 + D_3}} \left| \frac{z + c_1/\epsilon}{z - c_1/\epsilon} \right|^{\gamma/4c_1 D} \left| \frac{z + c_2/\epsilon}{z - c_2/\epsilon} \right|^{\gamma/4c_2 D}, \tag{50}$$

where

$$z = x - \frac{1}{2\epsilon}, \quad c_1 = \sqrt{i\epsilon\alpha + 1/4}, \quad c_2 = \sqrt{-i\epsilon\alpha + 1/4}, \quad \alpha = \sqrt{D_3/D}. \tag{51}$$

See Appendix B for the details of this derivation. Figure 6 shows examples of these solutions, for $D = 10$ and $D_3 = 10^{-2}$ to 10^{-5}. It is gratifying to note that the solutions are still bimodal, so this feature is preserved. Also, as one might expect, smaller D_3 yields peaks, at both the stable point e and the unstable point 0, that are both narrower and higher. It is worth explicitly noting though that the case without an additive noise ($D_3 = 0$) cannot be obtained by naively taking the limit of $D_3 \to 0$ in Eq. (50), as $D_3 \to 0$ is a singular limit [7]. Without additive noise stationary distributions simply do not exist, and the time-dependent PDF is given by Eq. (16). This is similar to the impossibility of recovering the Euler equation for the inviscid fluid from the Navier-Stokes equation for the viscous fluid by taking the limit of zero viscosity.

B. Numerical Solutions

For the Gompertz model the integrals that would be required to obtain the stationary solutions to Eq. (49) cannot be evaluated analytically. Also, if full time-dependent solutions are desired, then neither Eq. (48) nor (49) have analytic solutions. Numerical solvers to both the steady-state and time-dependent problems were developed, based on standard
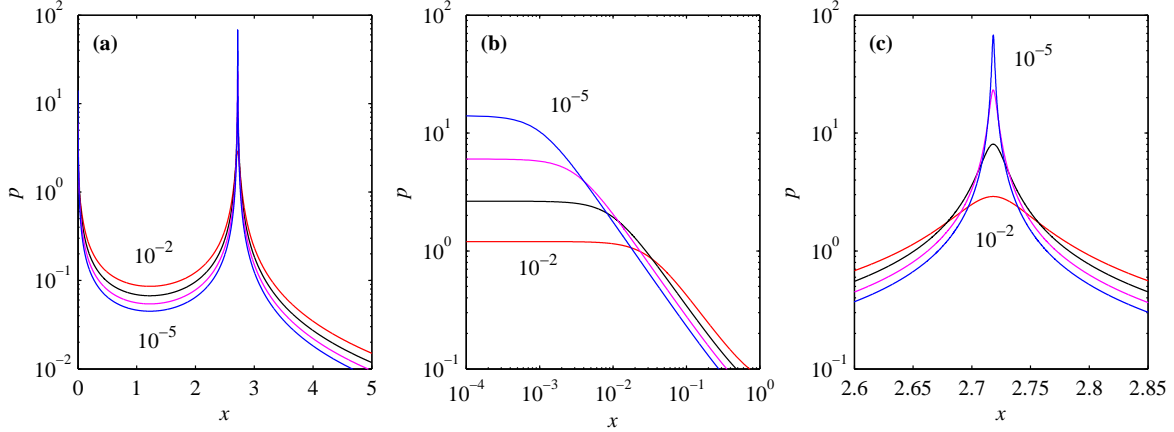
FIG. 6: All three panels show the same quantity, namely the logistic stationary distribution given by Eq. (50), with $D = 10$, and $D_3 = 10^{-2}$ to 10^{-5} as indicated. (a) shows the entire structure; note incidentally how $p(x)$ now extends into the region $x > e$ as well. (b) shows the details of the peak at 0, and (c) shows the peak at e.

finite-difference formulas. The results are second-order accurate in space, and also in time for the time-stepping version. Most aspects of these solvers are standard, so details are not presented. The only aspect that requires discussion are the associated boundary conditions. We begin by summarizing either of Eq. (48) or (49) in the generic form

$$\partial_t p = -\partial_z[F(z)p] + D\partial_z[G(z)\partial_z(G(z)p)] + D_3\partial_{zz}p, \tag{52}$$

where z represents either x or y, and the functions F and G are as appropriately defined for the two models. If we then integrate Eq. (52) between $z = 0$ and some upper boundary Z, we obtain

$$\frac{d}{dt}\int_0^Z p\,dz = (-Fp + D\,G\partial_z(Gp) + D_3\partial_z p)\Big|_0^Z. \tag{53}$$

Now, $F(0) = G(0) = 0$ for both logistic and Gompertz models, so this becomes

$$\frac{d}{dt}\int_0^Z p\,dz = (-Fp + D\,G\partial_z(Gp) + D_3\partial_z p)(Z) - D_3\partial_z p(0). \tag{54}$$

Certainly in the limit $Z \to \infty$ we require that the total probability integral should remain constant, so the boundary condition at $z = 0$ must be that $\partial_z p = 0$. Of course, $Z \to \infty$ cannot be achieved in any numerical solver; some finite upper boundary must always be chosen. In previous work on other Fokker-Planck equations [35, 36], the resulting PDFs dropped off sufficiently rapidly for large z (exponentially or even faster) that just imposing

21

$p(Z) = 0$ yielded excellent results, and conserved the total probability extremely well. Here though this approach was found not to work, and caused the integral $\int_0^Z p\,dz$ to decrease in time, even if Z as large as 100 was chosen. The reason is that here p decreases so slowly ($\sim 1/z^2$) for large z that unacceptably large values of Z would have to be chosen to make $p(Z)$ sufficiently small for $p(Z) = 0$ to be a reasonable approximation. Fortunately, Eq. (54) already provides the remedy: if the outer boundary condition is simply chosen to be

$$-Fp + D\,G\partial_z(Gp) + D_3\partial_z p = 0 \qquad \text{at} \quad z = Z, \tag{55}$$

then taking Z as small as 10 works very well, with the probability integral properly conserved. Spatial grids up to 10^7 grid points were used, and results were carefully checked to ensure they were independent of the grid size, time step, and precise choice of outer boundary Z.

C. Diagnostics of stationary distributions

The qualitative features of the Gompertz stationary distributions are the same as previously seen in Figure 6 for the logistic model. Figure 7 summarizes how the peaks and widths of the peaks behave in the two models, for D varying from 0.1 to 100, and $D_3 = 10^{-2}$ to 10^{-5}. We see that the amplitude of the main peak at e is very similar in both models, hardly varies with D, and scales with D_3 as $D_3^{-1/2}$. The amplitude at 0 is very small for $D < 1$, but rises rapidly thereafter. For the Gompertz model $D = 1$ is already sufficient to have a local maximum at the origin; for the logistic model $D \approx 1 - 2$ is required (depending on D_3). For $D = 100$ both models have peaks at the origin that are almost as large as the peaks at e. Unlike the previous Gompertz singularity at the origin though, there is now no case where the 0-peak exceeds the e-peak.

Turning next to the widths (which we define to be the width at half the peak amplitude), the variation with D_3 is as one might expect, namely $\sim D_3^{1/2}$, for all D. The variation with D is less obvious, indeed somewhat counter-intuitive. For $D \leq O(1)$ the widths of the peaks at e hardly vary with D, whereas for $D \geq O(1)$ they *decrease* as $D^{-1/2}$. That is, even though it is larger D which is causing the PDFs to spread out from the stable equilibrium point, in the immediate vicinity of e a larger D yields a narrower peak. The widths of the peaks at 0 show a similar $D^{-1/2}$ scaling in the $D \geq O(1)$ regime where they are peaks at all.

Figure 8 shows three further diagnostic quantities, all intended to measure the extent to
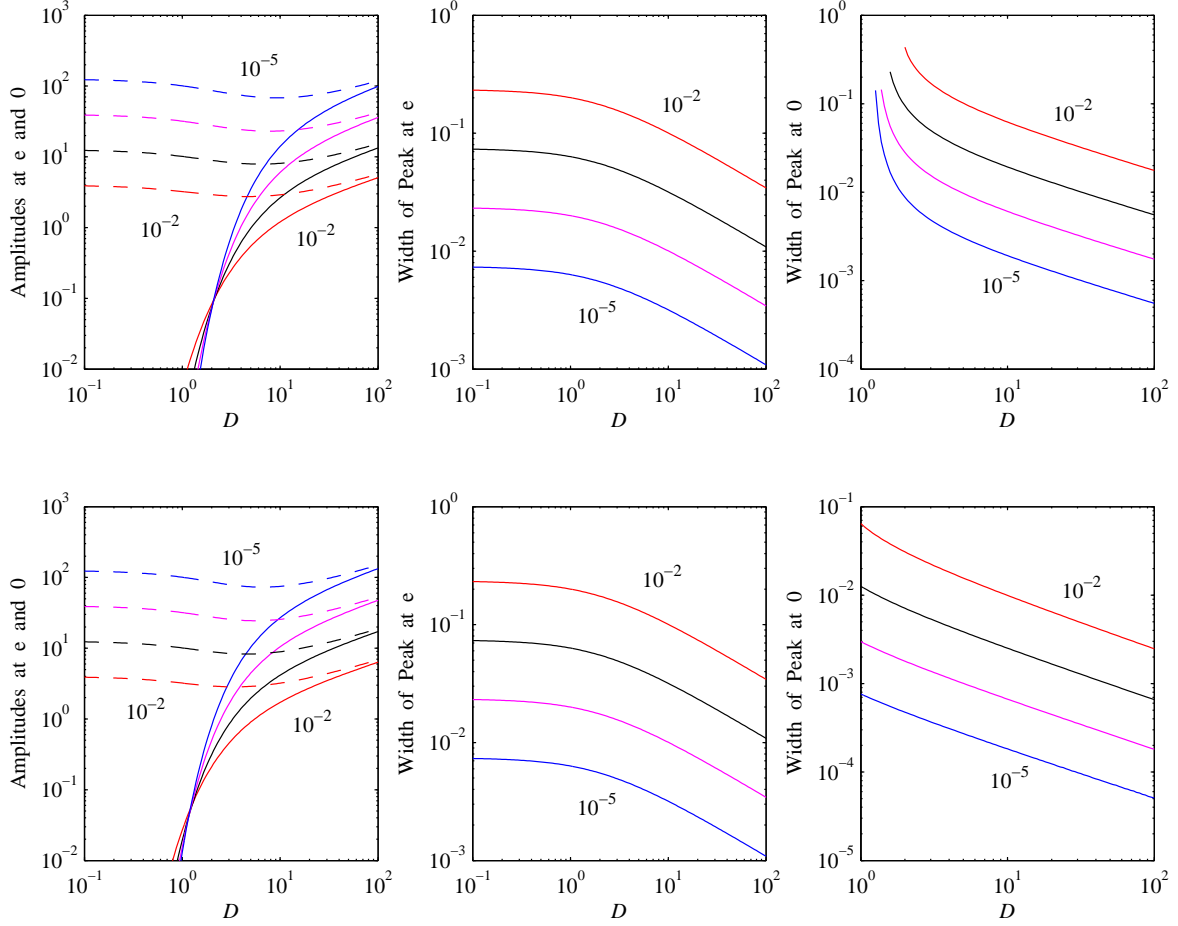
FIG. 7: The top row shows results for the logistic model, the bottom row for the Gompertz model. The first panel in each row shows the amplitudes $p(e)$ (dashed) and $p(0)$ (solid). $D_3 = 10^{-2}$ to 10^{-5} as indicated. The second panel in each row shows the widths at half-peak of the peaks at e, again for D_3 as indicated. The final panels show the widths at half-peak of the peaks at 0. Note how D here only covers a smaller range than in the other panels; for smaller D the origin is either not a peak at all, or not yet sufficiently dominant to have a corresponding half-peak.

which a PDF is localised versus spread out. First we have the familiar standard deviation σ, defined as

$$\sigma = \left(\int (z - \langle z \rangle)^2 p \, dz \right)^{1/2}, \quad \langle z \rangle = \int z p \, dz, \tag{56}$$

where z is either x for logistic or y for Gompertz. As long as D is sufficiently small that the PDFs are unimodal, σ is a good measure of localisation, measuring much the same (to within a multiplicative constant) as the widths at half-peak. Once the PDFs become bimodal
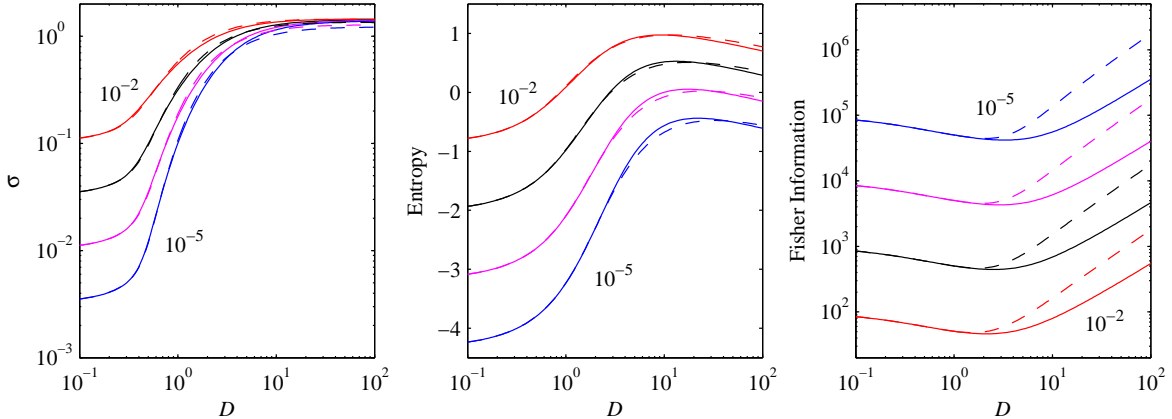
FIG. 8: From left to right plots of standard deviation σ, entropy and Fisher information as functions of D, for $D_3 = 10^{-2}$ to 10^{-5} as indicated. Solid lines show results for the logistic stationary distribution, dashed lines for Gompertz.

though, σ is largely useless, and is only measuring the distance between the two peaks rather than any details associated with either peak. Next we have the so-called differential entropy

$$S \propto - \int p \ln p \, dz, \qquad (57)$$

where the Boltzmann constant K_B is not shown explicitly. Eq. (57) is a measure of disorder and variability, and is thus expected to be small for highly localised PDFs and large for spread out ones (e.g. [35–37]). We see that entropy does a far better job than σ did of still distinguishing structures even in the bimodal regime; note how S continues to vary with both D and D_3 even in the regime where σ has become useless. Finally, another useful measure of information is the Fisher information

$$I = \int \frac{(\partial_z p)^2}{p} \, dz, \qquad (58)$$

which is expected to have the opposite behaviour as the entropy (e.g. [35–37]). We see that Fisher information again shows variation with D and D_3 even in the bimodal regime, where it also distinguishes the most between the two models. We conclude therefore that the most useful diagnostics of variability in bimodal structures are the Fisher information and then entropy, while σ is only capturing the distance between peaks but nothing else about the PDFs.

24

D. Time-dependent solutions

Finally, a substantial number of runs was done exploring how different initial conditions evolve toward the stationary distributions considered previously. It was found that logistic and Gompertz models behave similarly; only logistic results will therefore be presented in detail here. We start with the initial condition

$$p_0 = \sqrt{\frac{500}{\pi}}\, exp\left[-500(x - x_0)^2\right], \tag{59}$$

and varied x_0 in the range $(0.1, 4)$. The factor 500 was chosen to make the initial Gaussian peak slightly narrower but comparable to the expected final distributions. Taking even narrower initial conditions simply involves additional broadening, but otherwise qualitatively the same behaviour. Similarly, $D_3 = 0.01$ is fixed here; other values were explored, and yielded results generally similar, just with different widths as explored before for the stationary distributions.

Figure 9 shows results for the total information length $\mathcal{L}_\infty$ that occurred when starting from this initial condition (59) and evolving the solution to the final stationary distribution. We see how logistic and Gompertz models are indeed very similar. Both have $\mathcal{L}_\infty \approx O(10)$ for $D = 0.1$, 1 and 10. The dip around $x_0 \approx 0$ reflects that the multiplicative noise endows the certain degree of stability to the unstable equilibrium point (in the absence of the noise), making it more similar to the equilibrium point e; if the initial peak is already near its final position, then very little information change is needed to reach the final position. Alternatively, this suggests that the multiplicative noise induces fast switching between the stable and unstable equilibrium points.

Figure 10 shows the detailed spatial structures throughout the evolution, for the four representative cases $D = 0.1$ and 10, and $x_0 = 0.5$ and 4. Considering $D = 0.1$ first, the solutions always remain relatively narrow, as we might expect based on the previous results. The peaks move monotonically from x_0 to e; that is, $x_0 = 0.5$ moves outward, and $x_0 = 4$ moves inward. It is interesting to note though that in the intermediate stages there is also a certain amount of diffusive spreading in the opposite direction. That is, for $x_0 = 0.5$ the PDF in the region $x < 0.5$ grows at least temporarily (although never becoming the dominant peak), and similarly for $x_0 = 4$ the PDF in the region $x > 4$ grows temporarily.
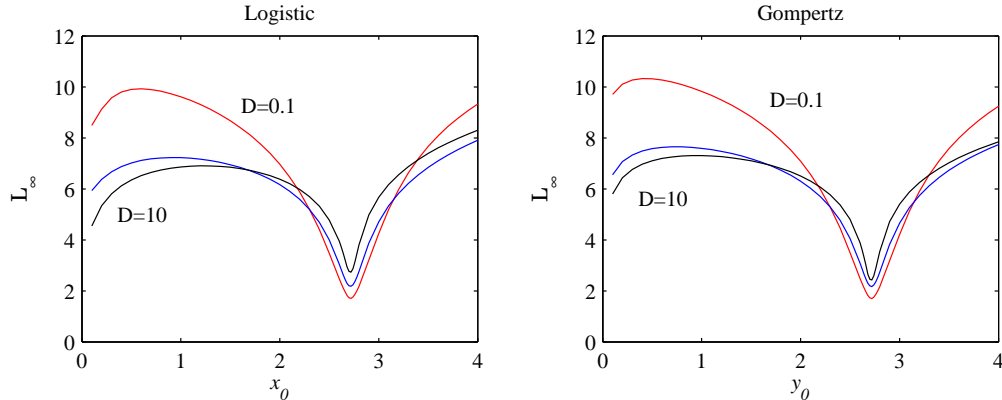
25

FIG. 9: $\mathcal{L}_\infty$ as a function of the initial peak position, for logistic on the left and Gompertz on the right. $D = 0.1$, 1 and 10 as indicated.

For $D = 10$ this movement away from the final position e is even more dramatic. For $x_0 = 0.5$ the peak itself moves toward 0, and it is only at later times that a new peak at e emerges and dominates. It was found that all peaks with small x_0 initially move toward 0, whereas peaks with larger x_0 immediately move toward e. The dividing line occurs near $x_0 \approx 1$, where $\mathcal{L}_\infty$ in Figure 9 also has its local maximum. For $x_0 = 4$ (and all $x_0 > e$) the peak always moves toward e, but at least temporarily there is also a very substantial contribution in the region $x > 4$. (These results were done with the computational outer boundary set to $Z = 25$, but thanks to the boundary condition (55), even $Z = 10$ already yields results that are essentially indistinguishable.)

Figure 11 shows some diagnostic quantities that can be computed for the time-dependent PDFs in Figure 10. In the top row we have two measures of position, namely the position of the peak itself, and the average value $\langle x \rangle = \int xp\,dx$. For $D = 0.1$ both quantities behave much the same, simply moving monotonically from x_0 to e. For $D = 10$ they behave quite differently. For $x_0 = 0.5$ the position of the peak is as we saw before in Figure 10; that is, it moves toward 0, until eventually a new peak emerges at e and suddenly becomes the dominant peak. This abrupt transition is related to the dip of $\mathcal{L}_\infty$ in Figure 9 for small x_0, reflecting a sudden switching between the unstable and stable equilibrium points. In contrast, $\langle x \rangle$ still evolves monotonically toward e. For $x_0 = 4$ the position of the peak moves monotonically toward e, again as seen in Figure 10. It is $\langle x \rangle$ which now does something unexpected, namely initially increase to values significantly greater than 4. The explanation
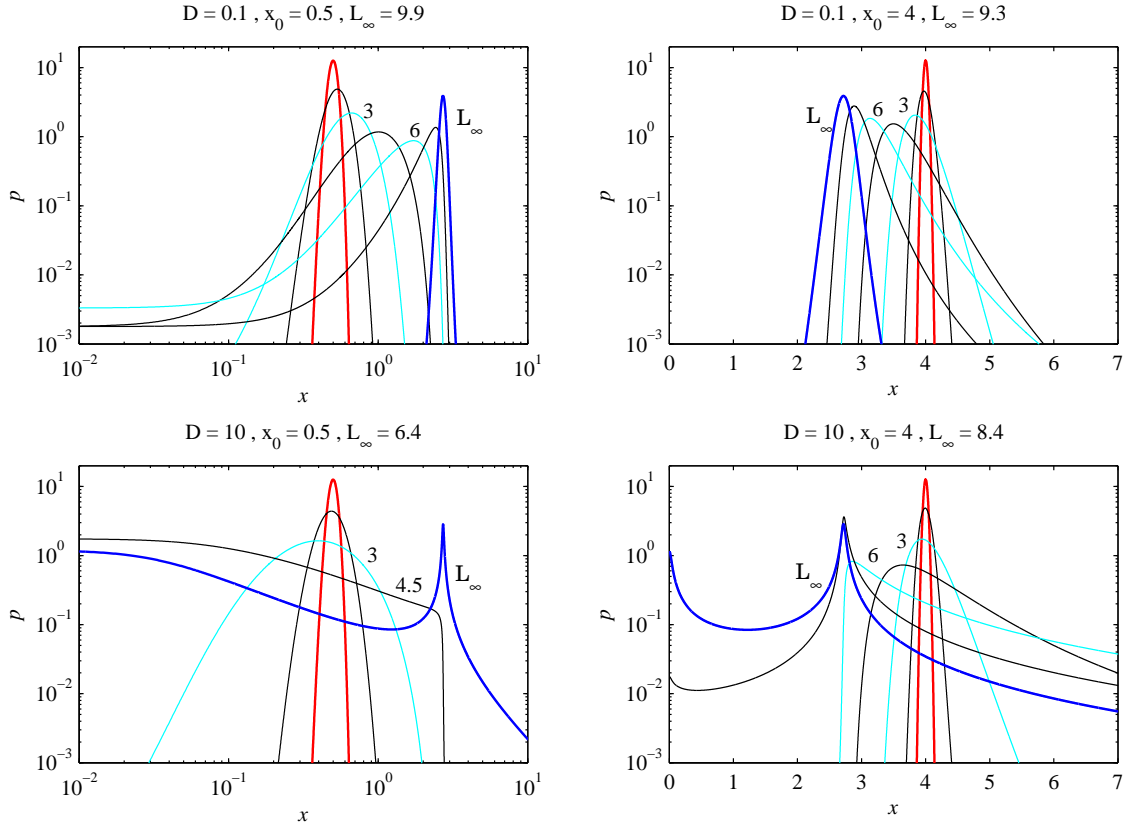
26

FIG. 10: Solutions of the logistic Fokker-Planck equation (48), with $D_3 = 0.01$ fixed, and $D = 0.1$ and 10, and $x_0 = 0.5$ and 4 as indicated. The initial condition (59) is the thick line peaking at the given x_0 value. The thick lines labelled $\mathcal{L}_\infty$ are the final stationary distributions, the same as previously in Eq. (50). The thin lines intermediate between initial and final states were chosen to have increments in $\mathcal{L}$ of 1.5, as indicated also by the numbers beside some of them.

of this is the phenomenon we saw before in Figure 10, that in the intermediate stages there is very significant diffusive spreading to the region $x > 4$, and at least initially the peak spreads far more toward $x > 4$ than toward $x < 4$.

Finally, the bottom row of Figure 11 shows the entropy (57), which is again seen to be a useful measure of how spread out the PDF is. In particular, the initial conditions (59) all start with $S \approx -2$, whereas the final values (which are the same as the corresponding results in Figure 8), are always greater, consistent with the fact that the final distributions are indeed more spread out than the initial conditions. We see though that in three of the four cases presented here, the entropy is not monotonic, indicating that at intermediate
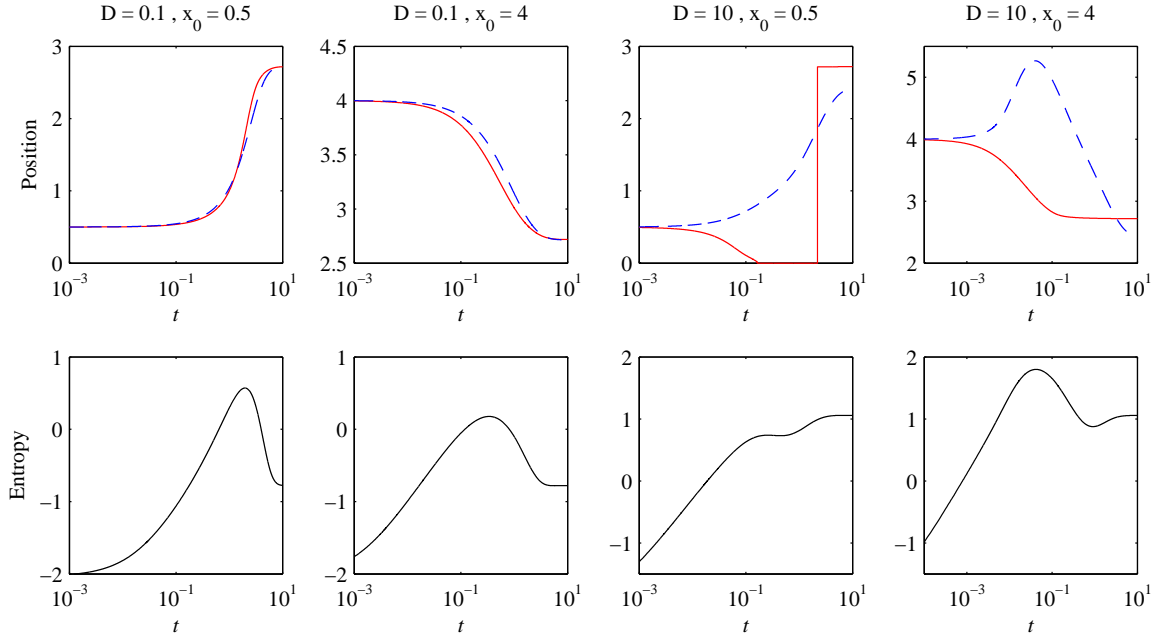
FIG. 11: The top row shows the position of the peak (solid) and the average value $\langle x \rangle$ (dashed) as functions of time, for the four logistic model solutions from Figure 10, as indicated. The bottom row shows corresponding results for the entropy $S(t)$.

stages of the evolution the PDFs are even more spread out.

VI. CONCLUSIONS

A growth model is widely used in understanding the dynamic evolution of populations, and two of the most popular models are the logistic and Gompertz models. The key difference between these two lies in different nonlinear damping, which is weaker in the Gompertz model than a quadratic damping in the logistic model. We examined consequences of this different nonlinear damping in attractor structure and time-evolution of stochastic logistic and Gompertz models by considering different types of stochastic noise. A stochastic noise D from a multiplicative (internal, e.g. epigenetic) source was shown to induce an interesting transition from unimodal to bimodal PDFs in both models as the attractor around the stable equilibrium point becomes leaky. A much weaker damping in the Gompertz model led to a much more significant (e.g. singular) growth of the population of a very small size around the unstable equilibrium point. Time-dependent PDFs were shown to be drastically different from stationary PDFs, while the variance is not a true representation

of the variability of a bimodal PDF, highlighting the importance of time-dependent PDFs. We also showed that the multiplicative noise can induce an abrupt switching between the unstable and stable equilibrium points.

These results can have an interesting implication for understanding the role of variability in experimentally observed bimodal distributions. For instance, comparing the distribution of inflammatory genes (experimentally observed to be bimodal) with house-keeping genes (experimentally observed to be unimodal) [6], we can infer that the variability in inflammatory genes is higher than that in house-keeping genes. Furthermore, our results imply that the maintenance of the population of small size is preferred as the stochastic component (e.g. epigenetic noise) in the growth rate dominates over the constant growth rate, as it happens in an environment very unfavourable for survival, for instance due to antibiotics or drugs. Our stochastic Gompertz model may be more relevant to the case of the extreme limit of a significant population of small size in such a scenario.

We also presented the information geometry associated with a growth process from the perspective of information change, and compare these two models in terms of the information length which represents the total number of statistically different states that the system undergoes in time. This information length provides a useful system-independent method of analyzing different stochastic processes to understand different experimental data. In particular, we showed that even though the time-evolutions of the two models are very different, they become more similar when measured in unit of the information length. These results suggest an interesting utility of the information length in unifying seemingly very different non-equilibrium growth processes.

Appendix A: Relation between $\mathcal{L}$ and relative entropy

We first show the relation between $\tau(t)$ in Eq. (48) and the second derivative of the relative entropy (or Kullback-Leibler divergence) $D(p_1, p_2) = \int dz\, p_2 \ln(p_2/p_1)$ where $p_1 = p(z, t_1)$

and $p_2 = p(z, t_2)$ as follows:

$$\frac{\partial}{\partial t_1} D(p_1, p_2) = -\int dz p_2 \frac{\partial_{t_1} p_1}{p_1}, \tag{A1}$$

$$\frac{\partial^2}{\partial t_1^2} D(p_1, p_2) = \int dz p_2 \left[\frac{(\partial_{t_1} p_1)^2}{p_1^2} - \frac{\partial_{t_1}^2 p_1}{p_1} \right], \tag{A2}$$

$$\frac{\partial}{\partial t_2} D(p_1, p_2) = \int dz \left[\partial_{t_2} p_2 + \partial_{t_2} p_2 (\ln p_2 - \ln p_1) \right], \tag{A3}$$

$$\frac{\partial^2}{\partial t_2^2} D(p_1, p_2) = \int dz \left[\partial_{t_2}^2 p_2 + \frac{(\partial_{t_2} p_2)^2}{p_2} + \partial_{t_2}^2 p_2 (\ln p_2 - \ln p_1) \right]. \tag{A4}$$

By taking the limit where $t_2 \to t_1 = t$ ($p_2 \to p_1 = p$) and by using the total probability conservation (e.g. $\partial_t \int dz p = 0$), Eqs. (A1) and (A3) above lead to

$$\lim_{t_2 \to t_1 = t} \frac{\partial}{\partial t_1} D(p_1, p_2) = \lim_{t_2 \to t_1 = t} \frac{\partial}{\partial t_2} D(p_1, p_2) = \int dz \partial_t p = 0,$$

while Eqs. (A2) and (A4) give

$$\lim_{t_2 \to t_1 = t} \frac{\partial^2}{\partial t_1^2} D(p_1, p_2) = \lim_{t_2 \to t_1 = t} \frac{\partial^2}{\partial t_2^2} D(p_1, p_2) = \int dz \frac{(\partial_t p)^2}{p}.$$

To link this to information length $\mathcal{L}$, we then express $D(p_1, p_2)$ for small $dt = t_2 - t_1$ as

$$D(p_1, p_2) = \left[\int dz \frac{(\partial_{t_1} p(z, t_1))^2}{p} \right] (dt)^2 + O((dt)^3), \tag{A5}$$

where $O((dt)^3)$ is higher order term in dt. We define the infinitesimal distance (information length) $dl(t_1)$ between t_1 and $t_1 + dt$ by

$$dl(t_1) = \sqrt{D(p_1, p_2)} = \sqrt{\int dz \frac{(\partial_t p)^2}{p}} dt + O((dt)^{3/2}). \tag{A6}$$

The total change in information between time 0 and t is then obtained by summing over $dt(t_1)$ and then taking the limit of $dt \to 0$ as

$$\begin{aligned} \mathcal{L}(t) &= \lim_{dt \to 0} \left[dl(0) + dl(dt) + dl(2dt) + dl(3dt) + \cdots dl(t - dt) \right] \\ &= \lim_{dt \to 0} \left[\sqrt{D(p(z, 0), p(z, dt))} + \sqrt{D(p(z, dt), p(z, 2dt))} + \cdots \sqrt{D(p(z, t - dt), p(z, t))} \right] \\ &\propto \int_0^t dt_1 \sqrt{\int dz \frac{(\partial_{t_1} p)^2}{p}}. \end{aligned} \tag{A7}$$

Appendix B: Derivation of stationary solution (50)

We look for the stationary solution of the Fokker-Planck equation Eq. (48)

$$0 = -\left[\gamma(x - \epsilon x^2)p\right] + D\left[x(1 - \epsilon x)\partial_x[x(1 - \epsilon x)p]\right] + D_3\partial_x p. \tag{B1}$$

We define $G(x) = x(1 - \epsilon x)$ and $F(x) = \gamma x(1 - \epsilon x)$ and express Eq. (B1) as

$$0 = -Fp + DG\partial_x[Gp] + D_3\partial_x p, \tag{B2}$$

$$\partial_x p[D_3 + DG^2] = p[F - DG\partial_x G], \tag{B3}$$

$$\partial_x p = p\frac{F}{D_3 + D_G^2} - \frac{1}{2}\frac{\partial_x[D_3 + DG^2]}{D_3 + DG^2}. \tag{B4}$$

The integral over x of the above equation gives us

$$p \propto \exp\left\{\int_{x_0}^{x} \frac{\gamma}{D}\frac{x'(1 - \epsilon x')}{\alpha^2 + x'^2(1 - \epsilon x')^2}dx' - \frac{1}{2}\ln\left[D_3 + Dx^2(1 - \epsilon x^2)\right]\right\}, \tag{B5}$$

where $\alpha^2 = D_3/D$. In order to compute Eq. (B5), we use the partial fraction decomposition

$$\frac{\gamma}{D}\frac{x(1 - \epsilon x)}{\alpha^2 + x^2(1 - \epsilon x)^2} = \sum_{i=1}^{4}\frac{k_i}{x - \omega_i}, \tag{B6}$$

where ω_i are the complex solutions of $\alpha^2 + x^2(1 - \epsilon x)^2$, which can be set as

$$\omega_i = \frac{1}{\epsilon}\left[\frac{1}{2} \pm \sqrt{\frac{1}{4} \pm i\epsilon\alpha}\right]. \tag{B7}$$

In the following, we let

$$c_1 = \sqrt{\frac{1}{4} + i\epsilon\alpha}, \qquad c_2 = \sqrt{\frac{1}{4} - i\epsilon\alpha}, \qquad y = x - \frac{1}{2\epsilon}. \tag{B8}$$

By using these notations, we compute the k_i and Eq. (B6) as

$$\frac{\gamma}{D}\frac{x(1 - \epsilon x)}{\alpha^2 + x^2(1 - \epsilon x)^2} = \frac{\gamma}{4Dc_1}\left[\frac{1}{y + c_1/\epsilon} - \frac{1}{y - c_1/\epsilon}\right] + \frac{\gamma}{4Dc_2}\left[\frac{1}{y + c_2/\epsilon} - \frac{1}{y - c_2/\epsilon}\right]. \tag{B9}$$

Thus, we obtain

$$\int_{x_0}^{x}\frac{\gamma}{D}\frac{x'(1 - \epsilon x')}{\alpha^2 + x'^2(1 - \epsilon x')^2}dx' \tag{B10}$$

$$= \int_{x_0}^{x}\frac{\gamma}{4Dc_1}\left[\frac{1}{y' + c_1/\epsilon} - \frac{1}{y' - c_1/\epsilon}\right] + \frac{\gamma}{4Dc_2}\left[\frac{1}{y' + c_2/\epsilon} - \frac{1}{y' - c_2/\epsilon}\right]dx' \tag{B11}$$

$$= \left[\frac{\gamma}{4Dc_1}\ln\frac{y' + c_1/\epsilon}{y' - c_1/\epsilon} + \frac{\gamma}{4Dc_2}\ln\frac{y' + c_2/\epsilon}{y' - c_2/\epsilon}\right]_{x_0}^{x}, \tag{B12}$$

31

which leads to Eq. (50).

---

[1] K. M. C. Tjorve and E. Tjorve, PLoS ONE **12** (6): e0178691, https://doi.org/10.1371/journal.pone.0178691 (2017).

[2] M. Kimura, J. Appl. Prob. **1**, 177-232 (1964).

[3] B.-q. Ai, X.-J. Wang, G.-T. Liu and L.-G. Liu, Phys. Rev. E. **67**, 022903 (2003); **77**, 013902 (2008).

[4] X.-M. Zhang and B.-q. Ai, Eur. Phys. J. B **73**, 433-437 (2010).

[5] C.-Y. Wang, Y. Gao, X.-W. Wang, Y.-M. Song, P. Zhou and H. Yang. Physica A **390**, 1-7 (2011).

[6] A. K. Shalek et al, Nature **510**, 363-369 (2014).

[7] A. Schenzle and H. Brand, Phys. Rev. A. **20**, 1628-1647 (1979).

[8] H. McAdams and A. Arkin, PNAS **94**, 814-819 (1997).

[9] D. Schultz, E. B. Jacob, J. N. Onuchic and P. G. Wolynes, PNAS **104**, 17582-17587 (2007).

[10] S. Levy, N. Ziv and M. Sigal, PLoS Biology **10**, e1001325 (2012).

[11] A. Sigal, et. al, Nature **444**, 643-646 (2006).

[12] J. Yokota, Carcinogenesis **21**, 497-503 (2000).

[13] D. Dingli, F. Michor, T. Antal and J.M. Pacheco, Cancer Biology & Theory **6:3**, 383-390 (2007).

[14] S.A. Frank and M.R. Rosner, PLoS Biology **10**, e1001296 (2012).

[15] G.C. Buehrling and R.R. Williams, Cancer Res. **36**, 3742-3747 (1976).

[16] E. Kim and J. Anderson, Phys. Plasmas **15**, 114506 (2008).

[17] E. Kim, H. Liu and J. Anderson, Phys. Plasmas **16**, 052304 (2009).

[18] A.P.L. Newton1, E. Kim and H.-L. Liu, Phys. Plasmas **20**, 092306 (2013).

[19] M. Tsuchiya, A. Giuliani, M. Hashimoto, J. Erenpreisa and K. Yoshikawa, PLoS One **10**, e0128565 (2015).

[20] H.J. Jensen, Self-organized criticality: emergent complex behavior in physical and biological systems (Cambridge Univ. Press, Cambridge, 1998).

[21] G. Pruessner, Self-organised criticality (Cambridge Univ. Press, Cambridge, 2012).

[22] G. Longo and M. Montévil, Progress in Biophysics and Molecular Biology. Systems Biology

and Cancer **106**, 340 (2011).

[23] S.W. Flynn, H.C. Zhao, and J.R. Green, J. Chem. Phys. **141**, 104107 (2014); J.W. Nichols, S.W. Flynn, J.R. Green, J. Chem. Phys., **142**, 064113 (2015).

[24] M.L. Ferguson, D. Le Coq, M. Jules, S. Aymerich, O. Radulescue, N. Declerck and C.A. Royer, PNAS **109**, 155 (2012).

[25] M. Ramirez et al, Nature Comm. **7**, 10690, doi:10.1038/ncomms10690 (2016)

[26] U. Lee , J. J. Skinner, J. Reinitz, M. R. Rosner, E. Kim, PLoS ONE **10** (7): e0132397, https://doi.org/10.1371/journal.pone.0132397 (2015).

[27] J. Heseltine and E. Kim, J. Phys. A **49**, 175002 (2016).

[28] E. Kim, U. Lee, J. Heseltine and R. Hollerbach, Phys. Rev. E **93**, 062127 (2016).

[29] F. Klebaner, Introduction to Stochastic Calculus with Applications (Imperial College Press, 2012).

[30] C. Gardiner, Stochastic methods, 4th Ed., (Springer, 2008).

[31] E. Wong and M. Zakai, Ann. Math. Stat. **36**, 1560 (1960).

[32] H. Risken, The Fokker-Planck Equation: Methods of Solution and Applications (Springer, Berlin, 1996).

[33] S.B. Nicholson and E. Kim, Phys. Lett. A. **379**, 8388 (2015).

[34] S.B. Nicholson and E. Kim, Entropy **18**, 258, e18070258 (2016).

[35] E. Kim and R. Hollerbach, Phys. Rev. E **95**, 022137 (2017).

[36] R. Hollerbach and E. Kim, Entropy **19**(6), 268, doi:10.3390/e1906026 (2017).

[37] B.R. Frieden, Physics from Fisher information (Cambridge Univ. Press, Cambridge, 2000).

[38] W.K. Wootters, Phys. Rev. D **23**, 357 (1981).

[39] G. Ruppeiner, Phys. Rev. A. **20**, 1608 (1979).

[40] P. Salamon. J.D. Nulton, G. Siragusa, A. Limon, D. Bedeaus and S. Kjelstrup, J. Non-Equilib. Thermodyn. **27**, 45 (2002).